Continuum Mech. Thermodyn. (2016) 28:215–234
DOI 10.1007/s00161-015-0420-y

ORIGINAL ARTICLE

Anil Misra · Payam Poorsolhjouy

Granular micromechanics based micromorphic model predicts frequency band gaps

Received: 10 December 2014 / Accepted: 2 March 2015 / Published online: 31 March 2015

Abstract Granular materials are typically characterized by complex structure and composition. Continuum modeling, therefore, remains the mainstay for describing properties of these material systems. In this paper, we extend the granular micromechanics approach by considering enhanced kinematic analysis. In this analysis, a decomposition of the relative movements of interacting grain pairs into parts arising from macro-scale strain as well as micro-scale strain measures is introduced. The decomposition is then used to formulate grain-scale deformation energy functions and derive inter-granular constitutive laws. The macro-scale deformation energy density is defined as a summation of micro-scale deformation energy defined for each interacting grain pair. As a result, a micromorphic continuum model for elasticity of granular media is derived and applied to investigate the wave propagation behavior. Dispersion graphs for different cases and different ratios between the microscopic stiffness parameters have been presented. It is seen that the model has the capability to present band gaps over a large range of wave numbers.

Keywords Granular materials · Micromechanics · Micromorphic continuum · Dispersion · Wave propagation

1 Introduction

Continuum modeling of granular media continues to be attractive and, arguably, the most feasible approach for describing their mechanical response at the macroscale. However, the imperatives of including the grain-scale information in macro-scale models have been widely recognized. The necessity of modeling micro-scale mechanisms in broader sense, within the rubric of continuum mechanics, is clear in the pioneering works of Cosserat [1], Mindlin [2], Toupin [3], Eringen [4], Green and Rivlin [5] and Germain [6]. Indeed, the early developments of continuum mechanics are known to proceed from some micromechanical conception of deformable materials (see Navier [7], Cauchy [8], and Piola [9,10]). For granular material systems, the grain-pair interactions and granular structures have a strong effect upon the collective behavior of grains. Consequently, approaches are needed that are different from the many micromechanical or multi-scale methods that have been conceived with the framework of continuum mechanics (see among others [11]). For example, the thermodynamics of granular materials can be described in the framework of mixtures [12] for the purpose of grain-size distribution evolution or of anisotropy evolution [13].

Here we follow the granular micromechanics approach which offers a robust methodology for developing continuum models of granular material systems by incorporating micro-scale effects [14–16]. This methodology considers grains and their interactions as the building block of the material and its macroscopic behavior.

Communicated by Victor Eremeyev, Peter Schiavone and Francesco dell'Isola.

A. Misra (✉) · P. Poorsolhjouy
Civil, Environmental and Architectural Engineering Department, University of Kansas,
1530 W. 15th Street, Learned Hall, Lawrence, KS 66045-7609, USA
E-mail: amisra@ku.edu

A continuum material point is therefore modeled as a granular volume element whose response is derived in terms of the meso-scale behavior of interacting grain pairs, orientation vectors, and average tensorial fabric measures. The granular micromechanics approach traces its genesis to the continuum models of grain packing developed in the second-half of the last century (see, for example, [17–22]). This approach has been applied to model a range of issues relevant to granular material behavior, including among others elastoplasticity [23], rate-dependent damage and plasticity [15,24], instability analysis [25,26] and second gradient and micro-polar effects [27–29], to give a small subset of contributions along these lines.

In this paper, the granular micromechanics approach is extended by considering the kinematic analyses of Mindlin–Eringen microstructural elasticity [2] or micromorphic mechanics [4]. The kinematics for a continuum material point is therefore enhanced by non-classical terms, including terms that model grain displacement fluctuations and higher gradients of deformations. The decomposition of interacting grain-pair relative displacement arising from different continuum kinematic variables in the kinematic analysis is then derived. The macro-scale stress measures conjugate to the introduced strain measures are defined by use of macro-scale deformation energy density. For granular material systems, the macro-scale deformation energy density is written as the volume average of grain-pair deformation energy. The macro-scale stress measures are, consequently, obtained in terms of the inter-granular force measures and the local geometry parameters. The micro-scale constitutive equations relating the inter-granular force and kinematic measures are then defined. As a result, macro-scale constitutive equations relating the stress measures to the strain measures are obtained in terms of the micro-scale stiffness coefficients and geometric properties. Further, the balance equations and displacement equations of motion for the derived theory are obtained and applied to investigate wave propagation phenomena. The resultant dispersion equations for different wave types are expressed in terms of the micro-scale properties to study the relationship between dispersion behavior and micro-scale parameters of granular media.

2 Kinematics of granular media

For the purpose of continuum modeling, consider a volume element (VE) of a granular media defined in the global coordinate system, $\boldsymbol{x}$. The displacement of grain, p, in this media can be expressed as a Taylor series expansion in terms of the displacement of neighboring grain, n, as follows

$$\phi_i^p = \phi_i^n + \phi_{i,j}^n l_j + \frac{1}{2}\phi_{i,jk}^n l_j l_k + \cdots \tag{1}$$

where ϕ_i is the displacement of grain centroids, l_j is an inter-granular branch vector joining the centroids of grains n and p, and the tensor product $l_j l_k (= J_{jk})$ is a geometry moment tensor. Terms of gradient up to second order have been included in the expansion. Summation convention over repeated indices is implied unless noted otherwise. In a continuum model, the VE plays the role of a material point P, as depicted in Fig. 1. A new coordinate system, $\boldsymbol{x'}$, is now attached to the material point P that can distinguish the different grains comprising P (see Fig. 1), such that the displacement of grain centroids can be denoted by $\phi_i(\boldsymbol{x},\boldsymbol{x'})$. The origin of $\boldsymbol{x'}$ is at the barycenter of P and moves with the displacement of P and its axes are parallel to coordinate system, $\boldsymbol{x}$.

Along the lines of the methodology of microstructural elasticity described by Mindlin [2] and micromorphic mechanics of Eringen [4], the displacement gradient, $\psi_{ij}(x_k) \overset{\Delta}{=} \phi_{i,j}(x_k)$, is decomposed as follows

$$\psi_{ij} \overset{\Delta}{=} \phi_{i,j} = \bar{\phi}_{i,j} - \gamma_{ij} \tag{2}$$

where $\bar{\phi}_{i,j}$ is the macro-scale displacement gradient independent of coordinates x_k, and $\gamma_{ij}(x_k)$ is the relative deformation. The second rank tensor $\gamma_{ij}(x_k)$ is interpreted as the gradient, with respect to the coordinates, x'_k, of the grain displacement fluctuations within the material point. The decomposition in Eq. 2, therefore, not only models the mean field grain displacements as in previous granular micromechanics theories [18–20], but also includes fluctuations in grain displacements as discussed in [30,31]. Since the second rank tensor $\gamma_{ij}(x_k)$ is independent of coordinates x'_k (homogeneous within the material point), the fluctuations modeled this way are taken as linear within the material point, which leads to a micromorphic theory of degree 1 in the terminology introduced by Germain [6]. The decomposition of displacement gradient in Eq. 2 is supported by the experimentally measured kinematic fields of grain assemblies [32–34] that show strong non-affine motions in a volume element comprising large number of grains. The presence of grain displacement fluctuations has

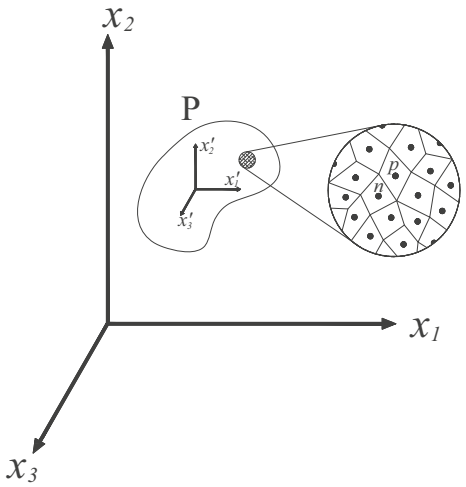

Fig. 1 Schematic of continuum material point, P, with its granular microstructure and the coordinate systems x and x'

also been recognized in previous works related to continuum modeling of grain packing within the rubric of classical continuum mechanics [30,35]. The second and higher gradient of deformations have also been shown to be necessary for continuum modeling of pantographic trusses due to their unique structural arrangements and stiffness of the truss elements [36,37] and also for bone mechanics [38]. The relative displacement of grains n and p can now be obtained by substituting Eq. 2 into Eq. 1 as follows

$$\delta_i^{np} = \phi_i^p - \phi_i^n = \left(\bar{\phi}_{i.j} - \gamma_{ij}\right) l_j + \frac{1}{2}\phi_{i,jk} l_j l_k = \bar{\phi}_{i,j} l_j - \gamma_{ij} l_j + \frac{1}{2}\phi_{i,jk} l_j l_k = \delta_i^M - \delta_i^m + \delta_i^g \tag{3}$$

where

$$\delta_i^M = \bar{\phi}_{i,j} l_j; \quad \delta_i^m = \gamma_{ij} l_j; \quad \delta_i^g = \frac{1}{2}\phi_{i,jk} l_j l_k = \phi_{i,jk} J_{jk} \tag{4}$$

As seen from Eq. 3, the inter-granular relative displacements between two interacting (contacting) grains are decomposed into three terms: (1) δ_i^M due to the average displacement gradient, $\bar{\phi}_{i,j}$, (2) δ_i^m due to the gradients of the fluctuation in grain displacement, γ_{ij} (x), and (3) δ_i^g due to the second gradient term, $\phi_{i,jk}$, which is same as the gradient of the relative deformations, $\gamma_{ij,k}$. A similar analysis could be done for the contact problem [39,40].

The rotation of grain p can also be written as a Taylor series expansion in terms of the rotation of neighboring grain, n, as follows

$$\kappa_i^p = \kappa_i^n + \kappa_{i,p}^n l_p \tag{5}$$

where κ_i is the grain rotation and terms of second order and higher are ignored. Further, the rotational field inside the material point P can be derived as the curl of the displacement field as

$$\kappa_i = e_{jki}\phi_{k,j} \tag{6}$$

where e_{jki} is the Levi Cevita permutation symbol, and the derivative is taken with respect to the local coordinates system ($\boldsymbol{x}$'). Combining Eqs. 5 and 6, the relative rotation of two interacting grains, n and p, denoted by θ_i, is then obtained as

$$\theta_i^{np} = \kappa_i^p - \kappa_i^n = \kappa_{i,p}^n l_p = e_{jki}\phi_{k,jp} l_p \tag{7}$$

The inter-granular relative rotations between two interacting grains are, thus, related to the second gradient term, $\phi_{i,jk}$. That grains undergo relative rotations are also known from measurements of kinematic fields in grain assembles [32,34].

3 Macro-scale and micro-scale dynamics

The macro-scale deformation energy density of the granular continua can now be defined as a function of the continuum kinematic measures as: $W = W\left(\bar{\phi}_{(i,j)}, \gamma_{ij}, \phi_{ij,k}\right)$. Consequently, the macro-scale stress components conjugate to these kinematic measures are obtained as

$$\tau_{ij} = \frac{\partial W}{\partial \bar{\phi}_{(i,j)}} = \frac{\partial W}{\partial \varepsilon_{ij}}; \quad \sigma_{ij} = \frac{\partial W}{\partial \gamma_{ij}}; \quad \mu_{ijk} = \frac{\partial W}{\partial \gamma_{ij,k}} \tag{8}$$

where τ_{ij}, σ_{ij}, and μ_{ijk} are Cauchy stress, relative stress, and double stress, respectively. For a granular material system, the macro-scale deformation energy density, W, can be written in terms of micro-scale deformation energy caused by the relative motion of interacting grain pairs. The micro-scale deformation energy, W^α, can be defined as follows for the αth interacting pair as a function of the micro-scale kinematic measures: $W^\alpha\left(\delta_i^M, \delta_i^m, \delta_i^g, \theta_i^u\right)$, where for simplicity of presentation the superscript α has been dropped from the micro-scale kinematic variables. The overall energy density of the RVE is then given as

$$W = \frac{1}{V}\sum_\alpha W^\alpha\left(\delta_i^M, \delta_i^m, \delta_i^g, \theta_i^u\right) \tag{9}$$

Further, the inter-granular force and moment conjugates are introduced as derivatives of micro-scale energy function, W^α, with respect to each of the inter-particle kinematic measures as:

$$\begin{aligned} &\frac{\partial W^\alpha}{\partial \delta_i^{\alpha\xi}} = f_i^{\alpha\xi}; \quad \text{where} \quad \xi : M, m, g \\ &\frac{\partial W^\alpha}{\partial \theta_i^{\alpha u}} = m_i^{\alpha u} \end{aligned} \tag{10}$$

Substituting Eq. 9 into Eq. 8, applying chain rule of differentiation and making use of Eqs. 4 and 10 lead to the following expressions for the macro-scale stress measures:

$$\left.\begin{aligned} \tau_{ij} &= \frac{\partial W}{\partial \varepsilon_{ij}} = \frac{1}{V}\sum_\alpha \frac{\partial W^\alpha}{\partial \delta_k^M}\frac{\partial \delta_k^M}{\partial \varepsilon_{ij}} \\ \frac{\partial \delta_k^M}{\partial \varepsilon_{ij}} &= \frac{\partial\left(\varepsilon_{kq} l_q^\alpha\right)}{\partial\left(\varepsilon_{ij}\right)} = \delta_{ik}\delta_{jq} l_q^\alpha = \delta_{ik} l_j^\alpha \end{aligned}\right\} \Rightarrow \tau_{ij} = \frac{1}{V}\sum_\alpha \frac{\partial W^\alpha}{\partial \delta_k^M}\delta_{ik} l_j^\alpha = \frac{1}{V}\sum_\alpha f_i^M l_j^\alpha \tag{11}$$

$$\left.\begin{aligned} \sigma_{ij} &= \frac{\partial W}{\partial \gamma_{ij}} = \frac{1}{V}\sum_\alpha \frac{\partial W^\alpha}{\partial \delta_k^m}\frac{\partial \delta_k^m}{\partial \gamma_{ij}} \\ \frac{\partial \delta_k^m}{\partial \gamma_{ij}} &= \frac{\partial\left(\gamma_{kq} l_q^\alpha\right)}{\partial \gamma_{ij}} = \delta_{ik}\delta_{jq} l_q^\alpha = \delta_{ik} l_j^\alpha \end{aligned}\right\} \Rightarrow \sigma_{ij} = \frac{1}{V}\sum_\alpha \frac{\partial W^\alpha}{\partial \delta_k^m}\delta_{ik} l_j^\alpha = \frac{1}{V}\sum_\alpha f_i^m l_j^\alpha \tag{12}$$

$$\left.\begin{aligned} \mu_{ijk} &= \frac{\partial W}{\partial \phi_{i,jk}} = \frac{1}{V}\sum_\alpha\left(\frac{\partial W^\alpha}{\partial \delta_l^g}\frac{\partial \delta_l^g}{\partial \phi_{i,jk}} + \frac{\partial W^\alpha}{\partial \theta_l^u}\frac{\partial \theta_l^u}{\partial \phi_{i,jk}}\right) \\ \frac{\partial \delta_l^g}{\partial \gamma_{i,jk}} &= \frac{\partial\left(\phi_{l,qr} J_{qr}^\alpha\right)}{\partial \phi_{i,jk}} = \delta_{il}\delta_{jq}\delta_{rk} J_{qr}^\alpha = \delta_{il} J_{jk}^\alpha \\ \frac{\delta \theta_l^u}{\partial \phi_{i,jk}} &= \frac{\partial\left(e_{rql}\phi_{q,rp} l_p^\alpha\right)}{\partial \phi_{i,jk}} = \delta_{iq}\delta_{jr}\delta_{pk} e_{rql} l_p^\alpha = e_{jil} l_k^\alpha \end{aligned}\right\} \Rightarrow \mu_{ijk} = \frac{1}{V}\left(\sum_\alpha \frac{\partial W^\alpha}{\partial \delta_l^g}\delta_{il} J_{jk}^\alpha + \sum_\alpha \frac{\partial W^\alpha}{\partial \theta_l^u} e_{jil} l_k^\alpha\right)$$

$$= \frac{1}{V}\left(\sum_\alpha f_i^g J_{jk}^\alpha + \sum_\alpha m_l^u e_{jil} l_k^\alpha\right) \tag{13}$$

Thus, the macro-scale stress measures have been defined in terms of the inter-granular force measures and the local geometry represented by the branch vector, l_j, and geometry moment tensor, J_{jk}. We observe that the inter-granular forces $f_i^{\alpha M}$, $f_i^{\alpha m}$, and $f_i^{\alpha g}$ are related to the Cauchy, the relative, and the double stresses, respectively. Further, the inter-granular moment $m_i^{\alpha u}$ is related to the double stress. In Eqs. 11–13, the superscript α has been dropped from the micro-scale kinematic and force measures.

4 Micro-scale and macro-scale constitutive equations

For formulating micro-scale constitutive equations that relates the micro-scale kinematic measures to the conjugate inter-granular force measures, it is beneficial to define a local Cartesian coordinate system for each interacting grain pair. This coordinate system is composed of a unit normal vector, $\boldsymbol{n}$, along the direction of inter-granular branch vector, l_i, and two orthogonal axes, $\boldsymbol{s}$ and $\boldsymbol{t}$, lying in the tangential plane between the two particles, defined as

$$\begin{aligned} n_i &= \langle \cos\theta, \sin\theta\cos\phi, \sin\theta\sin\phi \rangle \\ s_i &= \langle -\sin\theta, \cos\theta\cos\phi, \cos\theta\sin\phi \rangle \\ t_i &= \langle 0, -\sin\phi, \cos\phi \rangle \end{aligned} \tag{14}$$

The inter-granular force and moment vectors, as well as the displacement and rotation vectors, are decomposed into components along the axes of the local coordinate system. Thus, the micro-scale deformation energy, W^α, is written in the following simple form

$$W^\alpha = \sum_\xi f_n^{\alpha\xi}\delta_n^{\alpha\xi} + f_s^{\alpha\xi}\delta_s^{\alpha\xi} + f_t^{\alpha\xi}\delta_t^{\alpha\xi} + m_n^{\alpha u}\theta_n^{\alpha u} + m_s^{\alpha u}\theta_s^{\alpha u} + m_t^{\alpha u}\theta_t^{\alpha u}; \quad \xi : M, m, g \tag{15}$$

where the subscripts n, s, and t represent the components in the local coordinate system. The terms that cross-link the normal and tangential directions have been neglected for simplicity and subscripts do not follow the tensor summation convention. For linear isotropic elasticity, the following quadratic form of W^α, is formulated

$$\begin{aligned} W^\alpha = \frac{1}{2}\Bigg[\sum_\xi & K_n^{\alpha\xi}\left(\delta_n^{\alpha\xi}\right)^2 + K_w^{\alpha\xi}\left(\delta_s^{\alpha\xi}\right)^2 + K_w^{\alpha\xi}\left(\delta_t^{\alpha\xi}\right)^2 \\ & + G_n^{\alpha u}\left(\theta_n^{\alpha u}\right)^2 + G_w^{\alpha u}\left(\theta_s^{\alpha u}\right)^2 + G_w^{\alpha u}\left(\theta_t^{\alpha u}\right)^2 \Bigg]; \quad \xi : M, m, g \end{aligned} \tag{16}$$

where K and G represent the inter-granular stiffness parameters for forces and moments, respectively, and tensor summation convention is not applicable. Notably, the terms that cross-link the different micro-scale kinematic measures have been ignored for simplicity. The introduced grain-pair stiffness parameters define the force conjugates associated with different micro-scale kinematic measures that contribute to inter-granular relative displacements and rotations. These stiffness parameters do not represent the stiffness of two isolated interacting grains. In the derived model, we have introduced four types of inter-granular stiffness parameters, namely the average, the fluctuation, the second gradient, and the rotational, distinguished by their superscripts M, m, g, and u, respectively. In this case, the generic micro-scale constitutive equations, after dropping the aforementioned superscripts, can be written in matrix form as

$$\begin{Bmatrix} f_n \\ f_s \\ f_t \end{Bmatrix} = \begin{bmatrix} K_n & 0 & 0 \\ 0 & K_w & 0 \\ 0 & 0 & K_w \end{bmatrix} \begin{Bmatrix} \delta_n \\ \delta_s \\ \delta_t \end{Bmatrix}; \quad \begin{Bmatrix} m_n \\ m_s \\ m_t \end{Bmatrix} = \begin{bmatrix} G_n & 0 & 0 \\ 0 & G_w & 0 \\ 0 & 0 & G_w \end{bmatrix} \begin{Bmatrix} \theta_n \\ \theta_s \\ \theta_t \end{Bmatrix} \tag{17}$$

Utilizing the rotation tensor that relates the local **nst** coordinates with the global coordinates, the micro-scale constitutive equations and the stiffness matrices can be written as

$$\begin{aligned} f_i^{\alpha\xi} &= K_{ij}^{\alpha\xi}\delta_j^{\alpha\xi}; \quad K_{ij}^{\alpha\xi} = K_n^{\alpha\xi}n_in_j + K_w^{\alpha\xi}\left(s_is_j + t_it_j\right); \quad \text{where } \xi : \text{M, m, g} \\ m_i^{\alpha u} &= G_{ij}^{\alpha u}\theta_j^{\alpha u}; \quad G_{ij}^{\alpha u} = G_n^{\alpha u}n_in_j + G_w^{\alpha u}\left(s_is_j + t_it_j\right) \end{aligned} \tag{18}$$

By substituting the micro-scale constitutive equations, Eq. 18, into Eqs. 11–13, the macro-scale constitutive relationships are derived linking the macro-scale kinematic measures to their conjugate stress tensors as follows

$$\tau_{ij} = \frac{1}{V}\sum_{\alpha} f_i^M l_j^\alpha = \frac{1}{V}\sum_{\alpha} K_{ik}^M \delta_k^M l_j^\alpha = \frac{1}{V}\sum_{\alpha} K_{ik}^M \varepsilon_{kq} l_q^\alpha l_j^\alpha = \left(\frac{1}{V}\sum_{\alpha} K_{ik}^M l_l^\alpha l_j^\alpha\right)\varepsilon_{kl} = C_{ijkl}^M \varepsilon_{kl} \quad (19)$$

$$\sigma_{ij} = \frac{1}{V}\sum_{\alpha} f_i^m l_j^\alpha = \frac{1}{V}\sum_{\alpha} K_{ik}^m \delta_k^\alpha l_j^\alpha = \frac{1}{V}\sum_{\alpha} K_{ik}^m \gamma_{kl} l_l^\alpha l_j^\alpha = \left(\frac{1}{V}\sum_{\alpha} K_{ik}^m l_l^\alpha l_j^\alpha\right)\gamma_{kl} = C_{ijkl}^m \gamma_{kl} \quad (20)$$

$$\begin{aligned}\mu_{ijk} &= \frac{1}{V}\sum_{\alpha}\left(f_i^g J_{jk}^\alpha + m_l^u e_{jil} l_k\right) = \frac{1}{V}\sum_{\alpha}\left(K_{il}^g \delta_l^g J_{jk}^\alpha + G_{lm}^u \theta_m^u e_{jil} l_k\right) \\ &= \frac{1}{V}\sum_{\alpha}\left(K_{il}^g \phi_{l,mn} J_{mn}^\alpha J_{jk}^\alpha + G_{pq}^u e_{mlq} \phi_{l,mn} l_n e_{jip} l_k\right) \\ &= \left(\frac{1}{V}\sum_{\alpha} K_{il}^g J_{mn}^\alpha J_{jk}^\alpha + \frac{1}{V}\sum_{\alpha} G_{pq}^u e_{mlq} e_{jip} l_k l_n\right)\phi_{l,mn} = \left(A_{ijklmn}^g + A_{ijklmn}^u\right)\phi_{l,mn}\end{aligned} \quad (21)$$

It is notable that the derived constitutive relationships in Eqs. 19–21 are uncoupled as a consequence of the assumption made to ignore the coupling terms between the different kinematic measures in the micro-scale deformation energy, W^α, as given in Eq. 16. The inclusion of cross-linking between different microscopic kinematic and force measures will lead to coupling terms in the macro-scale constitutive equations. These coupling terms will include two additional fourth rank stiffness tensors that link the Cauchy stress to the relative deformation tensor and relative stress to the average strain tensor. Additionally, there will be fifth rank stiffness tensors that cross-link the third rank double stress to second rank strain measures (and second rank stress tensors to the second gradient of displacements). Since fifth rank isotropic tensors do not exist, the later will always be zero for isotropic continuum. More complete relationships that include the cross-linking terms will be pursued in future.

The summations in Eqs. 19–21 are over all grain-pair interactions within a material point. The quantities within the summation can be evaluated provided we know the grain-pair stiffness and branch vectors. In principle, these properties are different for every interacting grain pair. However, the spatial distribution of these properties within the material point is not known. It is notable though that the quantities within the summation are functions of the orientations of the branch vector, that can be written in terms of the direction cosines as given in Eq. 14, and the product of grain-pair stiffness and branch length. For describing the mean behavior of a random granular material, the micro-scale parameter, represented by the product of grain-pair stiffness and branch length, can be taken to be averages for a given branch vector. Since the micro-scale parameters are defined separately for different branch vector orientations, the method is naturally powerful for modeling anisotropic materials. Thus, the directional distribution of the inter-granular interactions plays an important role in defining the constitutive tensors. In order to approach the directional dependency in a systematic way, a directional density distribution function, $\xi(\theta, \phi)$, is introduced. This distribution function is intended to represent the directional dependence of number and stiffness of the interacting grain pairs. For isotropic materials, there is no directional preference, and the directional density distribution function can be simply written as

$$\xi(\theta, \phi) = \frac{1}{4\pi} \Rightarrow \int_\theta \int_\phi \xi \sin\theta \mathrm{d}\theta \mathrm{d}\phi = 1 \quad (22)$$

For describing materials with general inherent anisotropy, directional density distribution functions may be formulated as described in [13,18,41,42]. Considering the volume density of grain-pair interactions in a material point to be N_p, and assuming an average grain-pair stiffness within a solid angle $\mathrm{d}\Omega = \mathrm{d}\theta \sin\theta \mathrm{d}\phi$, the summations in Eqs. 19–21 can be converted to integrations in the following form:

$$C_{ijkl}^M = \frac{1}{V}\sum_{\alpha} K_{ik}^M l_l^\alpha l_j^\alpha = l^2 N_p \int_{\theta=0}^{\pi}\int_{\phi=0}^{2\pi}\left(K_{ik}^M n_j n_l\right)\xi \sin\theta \mathrm{d}\phi \mathrm{d}\theta \quad (23)$$

$$C_{ijkl}^m = \frac{1}{V}\sum_{\alpha} K_{ik}^m l_l^\alpha l_j^\alpha = l^2 N_p \int_{\theta=0}^{\pi}\int_{\phi=0}^{2\pi}\left(K_{ik}^m n_j n_l\right)\xi \sin\theta \mathrm{d}\phi \mathrm{d}\theta \quad (24)$$

$$A^{g}_{ijklmn} = \frac{1}{V}\sum_{\alpha} K^{g}_{il} J^{\alpha}_{mn} J^{\alpha}_{jk} = \frac{l^4 N_p}{4}\int_{\theta=0}^{\pi}\int_{\phi=0}^{2\pi}\left(K^{g}_{il} n_j n_k n_m n_n\right)\xi \sin\theta \mathrm{d}\phi \mathrm{d}\theta \tag{25a}$$

$$A^{u}_{ijklmn} = \frac{1}{V}\sum_{\alpha} G^{u}_{pq} e_{mlq} e_{jip} l_k l_n = l^2 N_p \int_{\theta=0}^{\pi}\int_{\phi=0}^{2\pi}\left(G^{u}_{pq} e_{lmq} e_{ijp} n_k n_n\right)\xi \sin\theta \mathrm{d}\phi \mathrm{d}\theta \tag{25b}$$

It can be seen from the above equations that the granular micromechanical view of the material behavior gives rise to three constitutive tensors. These include two fourth rank constitutive tensors, C^{M}_{ijkl} and C^{m}_{ijkl}, and a sixth rank constitutive tensor given as the sum of tensors, A^{g}_{ijklmn}, and A^{u}_{ijklmn}. The grain-pair stiffness parameters in these constitutive tensors are conceived in a statistical sense to describe the essential grain-scale mechanisms in a collective granular system and do not represent the behavior of two isolated interacting grains. This view is in contrast to the previous continuum models of granular media in which the grain-pair stiffness is often taken to be those of isolated interacting grains (see, for example, [27,28,30,31]). In the current model, these stiffness parameters function as the fundamental material properties, which are related to their measurable continuum counterparts. Needless to say, results of classical continuum model will be recovered if the fluctuation, the second gradient, and the rotational inter-granular stiffness parameters vanish. However, it is clear from the kinematic analyses presented here that these mechanisms should have nonvanishing contributions. The need for including the fluctuation and second gradient terms is supported by analyses of grain packing [30,35] as well as computer simulations and experiments of grain assemblies [32–34] that show strong non-affine motions in a volume element comprising large number of grains.

It is clear from Eqs. 23 and 24 that the tensors C^{M}_{ijkl} and C^{m}_{ijkl} are formally similar. The differences between the two are the grain-pair stiffness components. For isotropic elasticity, the following closed-form expressions can be obtained by integrating Eqs. 23 and 24:

$$\left.\begin{aligned} &C^{\alpha}_{iiii} = \tfrac{l^2 N_p}{15}\left(3K^{\alpha}_{n} + 2K^{\alpha}_{w}\right); \quad C^{\alpha}_{iijj} = \tfrac{l^2 N_p}{15}\left(K^{\alpha}_{n} - K^{\alpha}_{w}\right) \\ &C^{\alpha}_{ijij} = \tfrac{l^2 N_p}{15}\left(K^{\alpha}_{n} + 4K^{\alpha}_{w}\right) \quad C^{\alpha}_{ijji} = \tfrac{l^2 N_p}{15}\left(K^{\alpha}_{n} - K^{\alpha}_{w}\right); \quad \mathrm{i} \neq \mathrm{j} \\ &C^{\alpha}_{ijkl} = 0; \quad \text{otherwise} \end{aligned}\right\}; \quad \alpha = m, M \tag{26}$$

In Eq. 26, the subscripts take values 1, 2, or 3 and summation over repeated indices is not implied. It may be recalled from Eq. 8 that the second rank stress tensor τ_{ij} is defined as conjugate to the symmetric part of the displacement gradient; therefore, these symmetry conditions need to be imposed upon the stiffness tensor C^{M}_{ijkl}. The stiffness tensor can be decomposed into the following symmetric part

$$\begin{aligned} C^{M}_{iiii} &= \frac{l^2 N_p}{15}\left(3K^{M}_{n} + 2K^{M}_{w}\right); \quad C^{M}_{iijj} = \frac{l^2 N_p}{15}\left(K^{M}_{n} - K^{M}_{w}\right) \\ C^{M}_{(ij)(ij)} &= \frac{l^2 N_p}{30}\left(2K^{M}_{n} + 3K^{M}_{w}\right); \quad \mathrm{i} \neq \mathrm{j} \\ C^{M}_{ijkl} &= 0; \quad \text{otherwise} \end{aligned} \tag{27}$$

and an antisymmetric part, which is discarded for the remainder of this paper.

$$\begin{aligned} C^{M}_{[ij][ij]} &= \frac{l^2 N_p}{6}\left(K^{M}_{w}\right) \quad C^{M}_{[ij][ji]} = -\frac{l^2 N_p}{6}\left(K^{M}_{w}\right); \quad i \neq j \\ C^{M}_{ijkl} &= 0; \quad \text{otherwise} \end{aligned} \tag{28}$$

The components of the sixth rank tensors A^{g}_{ijklmn} and A^{u}_{ijklmn} defined in Eqs. 25a and 25b for isotropic elasticity are

$$
\begin{cases}
A^g_{111111} = A^g_{222222} = A^g_{333333} = l^4 N_p \frac{5K^g_n + 2K^g_w}{35} \\
A^g_{111122} = A^g_{111133} = A^g_{112112} = A^g_{113113} = A^g_{122111} = A^g_{133111} = A^g_{221221} = A^g_{222233} = A^g_{222211} = A^g_{223223} \\
= A^g_{233222} = A^g_{331331} = A^g_{332332} = A^g_{333311} = A^g_{333322} = A^g_{211222} = A^g_{311333} = A^g_{322333} = l^4 N_p \frac{3K^g_n + 4K^g_w}{105} \\
A^g_{111221} = A^g_{111313} = A^g_{112222} = A^g_{112211} = 3A^g_{112233} = 3A^g_{112332} = A^g_{113333} = A^g_{113311} = 3A^g_{113223} = 3A^g_{113322} \\
= A^g_{122221} = 3A^g_{122331} = 3A^g_{123231} = 3A^g_{123312} = A^g_{133331} = 3A^g_{133221} = A^g_{221111} = A^g_{221122} = 3A^g_{221133} \\
= 3A^g_{221331} = A^g_{222112} = A^g_{222332} = A^g_{223333} = A^g_{223322} = 3A^g_{223113} = 3A^g_{223311} = 3A^g_{231123} = 3A^g_{231321} \\
= A^g_{233332} = 3A^g_{233112} = A^g_{331111} = A^g_{331133} = 3A^g_{331122} = 3A^g_{331221} = A^g_{332222} = A^g_{332233} = 3A^g_{332112} \\
= 3A^g_{332211} = A^g_{333113} = A^g_{333223} = A^g_{211112} = 3A^g_{211332} = A^g_{311113} = 3A^g_{311223} = 3A^g_{312123} = 3A^g_{312231} \\
= A^g_{322223} = 3A^g_{322113} = l^4 N_p \frac{K^g_n - K^g_w}{35} \\
A^g_{122122} = 3A^g_{122133} = 3A^g_{123123} = A^g_{133133} = 3A^g_{133122} = 3A^g_{231213} = A^g_{233233} = 3A^g_{233211} = A^g_{211211} \\
= 3A^g_{211233} = A^g_{311311} = 3A^g_{311322} = 3A^g_{312312} = A^g_{322322} = 3A^g_{322311} = l^4 N_p \frac{K^g_n + 6K^g_w}{35} \\
A^g_{ijklmn} = A^g_{ikjlmn} = A^g_{ijklnm} = A^g_{ikjlnm} \\
A^g_{ijklmn} = 0; \quad \text{otherwise}
\end{cases}
\tag{29}
$$

$$
\begin{cases}
A^u_{121121} = A^u_{122122} = A^u_{123123} = A^u_{131131} = A^u_{133133} = A^u_{232232} = A^u_{233233} = \frac{l^2 N_p}{15}\left(G^u_n + 4G^u_w\right) \\
A^u_{132132} = A^u_{231231} = \frac{l^2 N_p}{15}\left(2G^u_n + 3G^u_w\right) \\
A^u_{121233} = A^u_{122313} = A^u_{123231} = A^u_{123312} = A^u_{131322} = A^u_{132213} = A^u_{132321} = A^u_{133212} = A^u_{231123} \\
= A^u_{231312} = A^u_{232311} = A^u_{233121} = A\frac{l^2 N_p}{15}\left(G^u_n - G^u_w\right) \\
A^u_{ijklmn} = -A^u_{jiklmn} = -A^u_{ijkmln} \\
A^u_{ijklmn} = 0; \quad \text{otherwise}
\end{cases}
\tag{30}
$$

The nonzero components of the sixth rank tensor A are same as that obtained in [43].

5 Variational principle and balance equations

For completeness of our presentation and harmony of notations, the variational principle and the balance equations are briefly discussed following the works of Mindlin [2] and Germain [6]. Utilizing the definitions in Eq. 8, the variation of the internal potential energy can be written as follows

$$
\begin{aligned}
\delta W &= \tau_{ij}\delta\varepsilon_{ij} + \sigma_{ij}\delta\gamma_{ij} + \mu_{ijk}\delta\phi_{i,jk} = \tau_{ij}\delta\bar{\phi}_{(i,j)} + \sigma_{ij}\left(\delta\bar{\phi}_{(i,j)} - \delta\phi_{i,j}\right) + \mu_{ijk}\delta\phi_{i,jk} \\
&= \left[\left(\tau_{ij} + \sigma_{ij}\right)\delta\bar{\phi}_i\right]_{,j} - \left(\tau_{ij} + \sigma_{ij}\right)_{,j}\delta\bar{\phi}_i - \sigma_{ij}\delta\psi_{ij} + \left(\mu_{ijk}\delta\psi_{ij}\right)_{,k} - \mu_{ijk,k}\delta\psi_{ij}
\end{aligned}
\tag{31}
$$

where Leibniz differentiation rule and Eq. 2 have been used. The variational of the macro-scale deformation energy functional can now be obtained utilizing Gauss's divergence theorem of integration as follows

$$
\begin{aligned}
\delta\mathcal{W} = \int_v \delta W \mathrm{d}V &= -\int_v \left(\tau_{ij} + \sigma_{ij}\right)_{,j}\delta\bar{\phi}_i \mathrm{d}V - \int_v \left(\mu_{ijk,k} + \sigma_{ij}\right)\delta\psi_{ij}\mathrm{d}V \\
&+ \int_s \left(\tau_{ij} + \sigma_{ij}\right)n_j\delta\phi_i \mathrm{d}S + \int_s \mu_{ijk}n_k\delta\psi_{ij}\mathrm{d}S
\end{aligned}
\tag{32}
$$

Further, following Mindlin [2,44], the variational of the kinetic energy functional can be written as,

$$
\delta\mathcal{T} = \int_o^t \delta T \mathrm{d}t = -\int_o^t \mathrm{d}t \int_V \left(\rho\ddot{\bar{\phi}}_i\delta\bar{\phi}_i + \frac{1}{3}\rho' d^2_{ik}\ddot{\phi}_{k,j}\delta\phi_{i,j}\right)\mathrm{d}V = -\int_o^t \mathrm{d}t \int_V \left(\rho\ddot{\bar{\phi}}_i\delta\bar{\phi}_i + \frac{1}{3}\rho' d^2_{ik}\ddot{\psi}_{kj}\delta\psi_{ij}\right)\mathrm{d}V
\tag{33}
$$

where ρ is the overall mass density, ρ' is the micro-scale mass density, and the superimposed dots indicate time derivative. According to Mindlin, $\boldsymbol{d}$ is a second rank tensor defined as

$$
d^2_{ij} = d_p d_q\left(\delta_{p1}\delta_{q1}l_{i1}l_{j1} + \delta_{p2}\delta_{q2}l_{i2}l_{j2} + \delta_{p3}\delta_{q3}l_{i3}l_{j3}\right) = d^2_{ji}
\tag{34}
$$

where d_i is equal to half of the length of the micro-volume in ith direction and l_{ij} is a matrix containing the direction cosines of the micro-volume with respect to the internal coordinate system, $\boldsymbol{x'}$. For micro-volumes with edges of length $2d$ parallel to the axes of $\boldsymbol{x'}$, we get

$$\begin{aligned} d_1 &= d_2 = d_3 = d \\ l_{ij} &= \delta_{ij} \end{aligned} \tag{35}$$

where δ_{ij} is the Kronecker delta. Finally, the variational of the external work done by (1) the long-range volumic (body) forces and moments and (2) the contact surface forces and moments is defined as

$$\delta \mathcal{W}^{ext} = \int_v f_i \delta \bar{\phi}_i \mathrm{d}V + \int_v \Phi_{ij} \delta \psi_{ij} \mathrm{d}V + \int_s t_i \delta \bar{\phi}_i \mathrm{d}S + \int_s T_{ij} \delta \psi_{ij} \mathrm{d}S \tag{36}$$

In Eq. 36, f_i is the non-contact volumic (body) force per unit volume, t_i is the contact traction defined as a surface force per unit area, Φ_{ij} is the non-contact volumic (body) double force per unit volume, and T_{ij} is the contact double traction defined as double force per unit area. Now utilizing the action functional, the variational equation of motion is written using Hamilton's principle as

$$\delta A = \int_0^t \int_v (\delta T - \delta W) \, \mathrm{d}V \mathrm{d}t + \int_0^t \delta \mathcal{W}^{ext} \mathrm{d}t = \int_0^t \left(\delta \mathcal{W}^{ext} - \delta \mathcal{W} + \delta \mathcal{T} \right) \mathrm{d}t = 0 \tag{37}$$

Using Eqs. 32, 33, 36, and 37 yields the following after dropping the integration over time

$$\begin{aligned} \delta A = &\int_v \left[f_i + \left(\tau_{ij} + \sigma_{ij} \right)_{,j} - \rho \ddot{\bar{\phi}}_i \right] \delta \bar{\phi}_i \mathrm{d}V + \int_v \left[\Phi_{i,j} + \left(\mu_{ijk,k} + \sigma_{ij} \right) - \frac{1}{3} \rho' d_{ik}^2 \ddot{\psi}_{kj} \right] \delta \psi_{ij} \mathrm{d}V \\ &+ \int_s \left[t_i - \left(\tau_{ij} + \sigma_{ij} \right) n_j \right] \delta \bar{\phi}_i \mathrm{d}S + \int_s \left[T_{ij} - \mu_{ijk} n_k \right] \delta \psi_{ij} \mathrm{d}S = 0 \end{aligned} \tag{38}$$

Since Eq. 38 should hold for any arbitrary kinematic measures, for the action functional to be always identically zero, all integrands should vanish. This will lead to two balance equations stated in terms of the stress measures as

$$\left(\tau_{ij} + \sigma_{ij} \right)_{,j} + f_i = \rho \ddot{\bar{\phi}}_i \tag{39a}$$

$$\mu_{ijk,i} + \sigma_{jk} + \Phi_{jk} = \frac{1}{3} \rho' d^2 \ddot{\psi}_{jk} \tag{39b}$$

and two boundary conditions given in terms of the stress measures as

$$\left(\tau_{ij} + \sigma_{ij} \right) n_j = t_i \tag{40a}$$

$$\mu_{ijk} n_k = T_{jk} \tag{40b}$$

6 Identification of Mindlin's model using granular micromechanics

The constitutive relationships derived using the granular micromechanics approach can be identified with the constitutive coefficients introduced by Mindlin [2] and Eringen [4] from purely continuum viewpoint. We follow Mindlin's model which includes the following constitutive equations neglecting the coupling terms of his formulation to compare with the model derived in this paper

$$\begin{aligned} \tau_{ij} &= C_{ijkl} \varepsilon_{kl} \\ \sigma_{ij} &= B_{ijkl} \gamma_{kl} \\ \mu_{ijk} &= A_{ijklmn} \kappa_{lmn} \end{aligned} \tag{41}$$

where the stiffness tensors are defined as

$$\begin{aligned} C_{ijkl} &= \lambda \delta_{ij} \delta_{kl} + \mu \left(\delta_{ik} \delta_{jl} + \delta_{il} \delta_{jk} \right) \\ B_{ijkl} &= b_1 \delta_{ij} \delta_{kl} + b_2 \delta_{ik} \delta_{jl} + b_3 \delta_{il} \delta_{jk} \\ A_{ijklmn} &= a_1 \delta_{ij} \delta_{kl} \delta_{mn} + a_2 \delta_{ij} \delta_{km} \delta_{nl} + a_3 \delta_{ij} \delta_{kn} \delta_{ml} + a_4 \delta_{jk} \delta_{il} \delta_{mn} + a_5 \delta_{jk} \delta_{im} \delta_{nl} \\ &\quad + a_6 \delta_{jk} \delta_{in} \delta_{lm} + a_7 \delta_{ki} \delta_{jl} \delta_{mn} + a_8 \delta_{ki} \delta_{jm} \delta_{nl} + a_9 \delta_{ki} \delta_{jn} \delta_{lm} + a_{10} \delta_{il} \delta_{jm} \delta_{kn} \\ &\quad + a_{11} \delta_{jl} \delta_{km} \delta_{in} + a_{12} \delta_{kl} \delta_{im} \delta_{jn} + a_{13} \delta_{il} \delta_{jn} \delta_{km} + a_{14} \delta_{jl} \delta_{kn} \delta_{im} + a_{15} \delta_{kl} \delta_{in} \delta_{jm} \end{aligned} \tag{42}$$

The identification of the constitutive coefficients of Mindlin's model with those derived from the granular micromechanics approach can be easily achieved by comparing the components of C_{ijkl}, B_{ijkl}, and A_{ijklmn} with those of C^M_{ijkl}, C^m_{ijkl}, and A^u_{ijklmn} and A^g_{ijklmn}. Remarkably, the nonzero components in Mindlin's stiffness tensors are same as the nonzero components derived from the present model, and the following relationships between Mindlin's coefficients and inter-granular stiffness measures are found

$$\begin{cases} \lambda = \frac{l^2 N_p}{15}\left(K^M_n - K^M_w\right) \\ \mu = \frac{l^2 N_p}{30}\left(2K^M_n + 3K^M_w\right) \end{cases} \tag{43a}$$

$$\begin{cases} b_1 = b_3 = \frac{l^2 N_p}{15}\left(K^m_n - K^m_w\right) \\ b_2 = \frac{l^2 N_p}{15}\left(K^m_n + 4K^m_w\right) \end{cases} \tag{43b}$$

$$\begin{cases} a_1 = a_2 = a_3 = a_6 = a_9 = \frac{l^4 N_p}{105}\left(K^g_n - K^g_w\right) \\ a_4 = a_{13} = \frac{l^2 N_p}{105}\left(7\left(-G^u_n + G^u_w\right) + l^2\left(K^g_n + 6K^g_w\right)\right) \\ a_5 = a_7 = a_{11} = a_{12} = \frac{l^2 N_p}{105}\left(7\left(G^u_n - G^u_w\right) + l^2\left(K^g_n - K^g_w\right)\right) \\ a_8 = a_{15} = \frac{l^2 N_p}{105}\left(7\left(-G^u_n + G^u_w\right) + l^2\left(K^g_n - K^g_w\right)\right) \\ a_{10} = \frac{l^2 N_p}{105}\left(7\left(3G^u_n + 2G^u_w\right) + l^2\left(K^g_n + 6K^g_w\right)\right) \\ a_{14} = \frac{l^2 N_p}{105}\left(7\left(-3G^u_n - 2G^u_w\right) + l^2\left(K^g_n - K^g_w\right)\right) \end{cases} \tag{43c}$$

To illustrate the effects of the inter-granular stiffness coefficients on the macro-scale properties, the following ratios between tangential and normal components of inter-granular stiffness measures are defined.

$$\beta_M = \frac{K^M_w}{K^M_n}; \quad \beta_m = \frac{K^m_w}{K^m_n}; \quad \beta_g = \frac{K^g_w}{K^g_n} \quad \beta_G = \frac{G^u_w}{G^u_n} \tag{44}$$

It is usually assumed that normal components of the inter-granular stiffness are larger than their corresponding tangential values and they are both nonnegative. So these ratios are varied in the interval from 0 to 1. In Fig. 2, macro-scale constitutive coefficients are plotted as functions of their corresponding inter-granular stiffness measures. For the fourth rank stiffness tensors, the coefficients in Eqs. 43a–43c are presented while for the sixth rank stiffness tensor, the nonzero components provided in Eqs. 29 and 30 are shown. The sixth rank stiffness tensors from Mindlin can be derived using the presented components of A^u_{ijklmn} and A^g_{ijklmn}.

7 Displacement equations of motion and wave propagation

The derived model is applied to study the influence of micro-scale parameters upon wave propagation in an infinite medium. The displacement equations of motion are obtained by substituting the constitutive equations, Eqs. 19–21, into the balance equation, Eqs. 39a and 39b to find:

$$\left(C^M_{ijkl} + C^m_{ijkl}\right)\bar{\phi}_{k,lj} - C^m_{ijkl}\psi_{kl,j} = \rho\ddot{\bar{\phi}}_i \tag{45a}$$

$$\left(A^g_{ijklmn} + A^u_{ijklmn}\right)\psi_{lm,ni} + C^m_{jklm}\bar{\phi}_{l,m} - C^m_{jklm}\psi_{lm} = \frac{1}{3}\rho' d^2 \ddot{\psi}_{jk} \tag{45b}$$

where the non-contact volumic forces and double forces, f_i and Φ_{ij}, are assumed to be absent. Without loss of generality, we investigate the propagation of waves along x_1 axis. In this case for a plane wave solution, all kinematic measures should be only functions of x_1 [45]

$$\begin{aligned} \bar{\phi}_i &= \bar{\phi}_i\left(x_1, t\right) \\ \psi_{ij} &= \psi_{ij}\left(x_1, t\right) \end{aligned} \tag{46}$$

There are altogether twelve equations of motion in terms of the three average displacement field variables, $\bar{\phi}_i$, and nine micro-displacement gradient field variables, ψ_{ij}. For isotropic media, these twelve equations can be decomposed into three independent equations plus three systems of three equations and three unknowns by

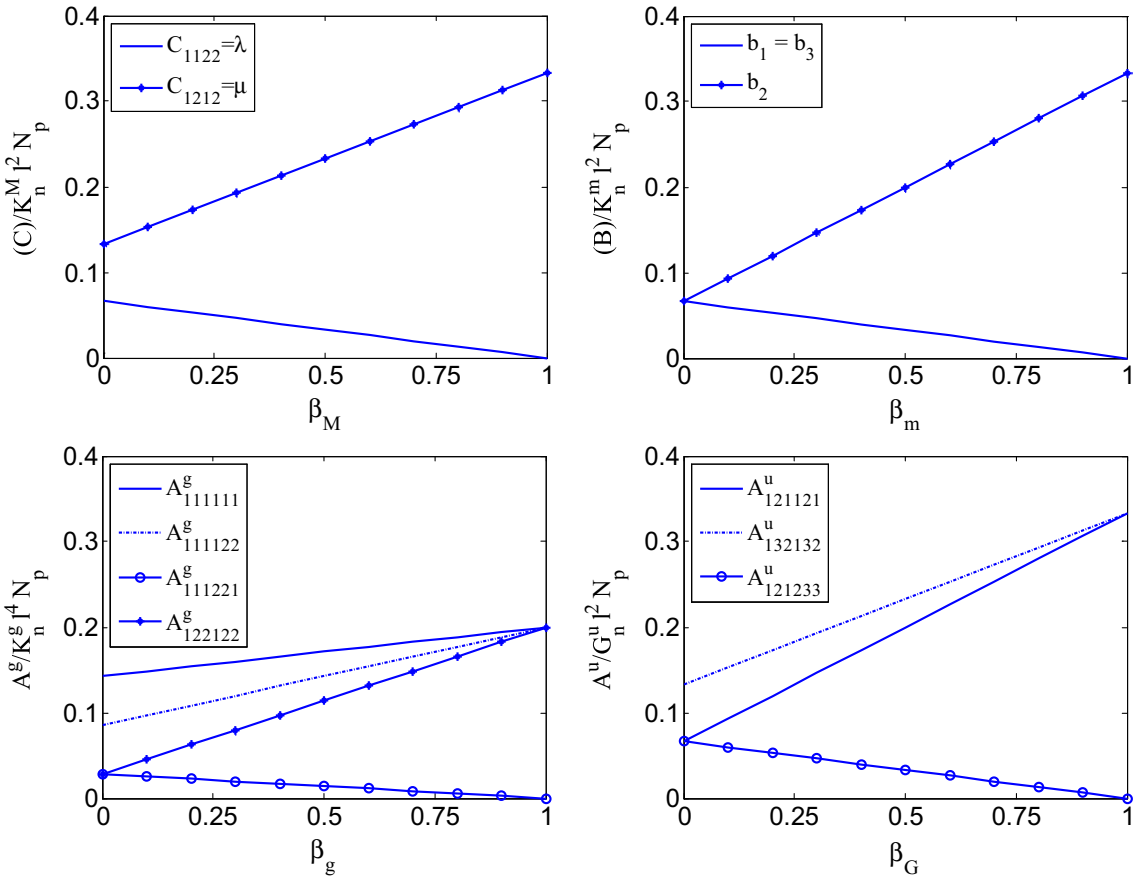

Fig. 2 Normalized macro-scale constitutive coefficients shown as functions of the ratio between normal and tangential components of the micro-scale stiffness parameters

using linear combination following Mindlin [2]. To this end, the second rank tensor ψ_{ij} is decomposed into a volumetric part, a skew-symmetric part, and a deviatoric part as follows

$$\psi_{ij} = \frac{1}{3}\psi_{kk}\delta_{ij} + \psi_{[ij]} + \left(\psi_{(ij)} - \frac{1}{3}\psi_{kk}\delta_{ij}\right) = \psi^V_{ij} + \psi^S_{ij} + \psi^D_{ij} \tag{47}$$

where $\psi^V_{ij} = \frac{1}{3}\psi_{kk}\delta_{ij}$ is the volumetric part, $\psi^S_{ij} = \psi_{[ij]}$ is the skew-symmetric part, and $\psi^D_{ij} = \psi_{(ij)} - \frac{1}{3}\psi_{kk}\delta_{ij}$is the deviatoric part. The twelve separated equations of motion include two uncoupled equations for two transverse shear waves and one for a transverse rotational wave

$$(a_{10} + a_{13})\,\psi_{(23),11} - (b_2 + b_3)\,\psi_{(23)} = \frac{1}{3}\rho' d^2 \ddot{\psi}_{(23)} \tag{48a}$$

$$(a_{10} + a_{13})\left(\psi_{22,11} - \psi_{33,11}\right) - (b_2 + b_3)\left(\psi_{22} - \psi_{33}\right) = \frac{1}{3}\rho' d^2\left(\ddot{\psi}_{22} - \ddot{\psi}_{33}\right) \tag{48b}$$

$$(a_{10} - a_{13})\,\psi_{[23],11} - (b_2 - b_3)\,\psi_{[23]} = \frac{1}{3}\rho' d^2 \ddot{\psi}_{[23]} \tag{48c}$$

Other equations will not be in the decomposed fashion like Eqs. 48a–48c. These will include one system of equations for longitudinal waves

$$\begin{cases} k_{11}\bar{\phi}_{1,1} - k_{12}\psi^D_{11,1} - k_{13}\psi^V_{,1} = \rho\ddot{\bar{\phi}}_1 \\ k_{21}\bar{\phi}_{1,1} + k_{22}\psi^D_{11,11} - k'_{22}\psi^D_{11} + k_{23}\psi^V_{,11} = \frac{1}{2}\rho' d^2 \ddot{\psi}^D_{11} \\ k_{31}\bar{\phi}_{1,1} + k_{32}\psi^D_{11,11} + k_{33}\psi^V_{,11} - k'_{33}\psi^V = \rho' d^2 \ddot{\psi}^V \end{cases} \tag{49}$$

and two sets of equations for transverse waves

$$\left.\begin{array}{l}\bar{k}_{11}\bar{\phi}_{\xi,11}-\bar{k}_{12}\psi_{(1\xi),1}-\bar{k}_{13}\psi_{[1\xi],1}=\rho\ddot{\bar{\phi}}_{\xi}\\ \bar{k}_{21}\bar{\phi}_{\xi,1}+\bar{k}_{22}\psi_{(1\xi),11}-\bar{k}'_{22}\psi_{(1\xi)}+\bar{k}_{23}\psi_{[1\xi],11}=\frac{2}{3}\rho' d^2\ddot{\psi}_{(1\xi)}\\ \bar{k}_{31}\bar{\phi}_{\xi,1}+\bar{k}_{32}\psi_{(1\xi),11}+\bar{k}'_{33}\psi_{[1\xi],11}-\bar{k}_{33}\psi_{[1\xi]}=\frac{2}{3}\rho' d^2\ddot{\psi}_{[1\xi]}\end{array}\right\};\ \xi=2\text{ and }3 \tag{50}$$

The stiffness constants used in Eq. 49, k_{ij}, and k'_{ij}, derived in terms of the micro-scale stiffness components used in this model are given as

$$\begin{aligned}k_{11}&=\frac{l^2N_p}{15}\left[\left(3K_n^m+2K_w^m\right)+\left(3K_n^M+2K_w^M\right)\right]\\ k_{22}&=\frac{l^2N_p}{105}\left[l^2\left(11K_n^g+10K_w^g\right)+15G_w^u\right]\\ k_{33}&=\frac{l^2N_p}{3}\left[l^2\left(K_n^g+2K_w^g\right)+2G_w^u\right]\\ k_{23}=k_{32}&=\frac{l^2N_p}{15}\left[2l^2\left(K_n^g-K_w^g\right)-5G_w^u\right]\\ k_{13}=k_{31}&=\frac{l^2N_p}{3}K_n^m\\ k_{12}=k_{21}&=\frac{l^2N_p}{15}\left(2K_n^m+3K_w^m\right)\\ k'_{22}&=\frac{l^2N_p}{10}\left(2K_n^m+3K_w^m\right)\\ k'_{33}&=l^2N_pK_n^m\end{aligned} \tag{51}$$

and the ones used in Eq. 50, $\bar{k}_{ij}$, and $\bar{k}'_{ij}$, are

$$\begin{aligned}\bar{k}_{11}&=\frac{l^2N_p}{15}\left[\left(K_n^m+4K_w^m\right)+\left(K_n^M+1.5K_w^M\right)\right]\\ \bar{k}_{22}&=\frac{l^2N_p}{105}\left[l^2\left(12K_n^g+16K_w^g\right)+7\left(G_n^u+4G_w^u\right)\right]\\ \bar{k}_{33}&=\frac{l^2N_p}{15}\left(G_n^u+4G_w^u\right)\\ \bar{k}_{23}=k_{32}&=\frac{l^2N_p}{15}\left[l^2K_w^g+\left(G_n^u-G_w^u\right)\right]\\ \bar{k}_{13}=k_{31}&=\frac{l^2N_p}{3}K_w^m\\ \bar{k}_{12}=k_{21}&=\frac{l^2N_p}{15}\left(2K_n^m+3K_w^m\right)\\ \bar{k}'_{22}&=\frac{l^2N_p}{15}\left(4K_n^m+6K_w^m\right)\\ \bar{k}'_{33}&=\frac{2l^2N_p}{3}K_w^m\end{aligned} \tag{52}$$

Harmonic wave functions given below serve as solutions to the above set of equations (Eqs. 48a–48c)

$$\begin{aligned}\bar{\phi}_i&=A_i i\exp\left[i\left(\xi x_1-\omega t\right)\right]\\ \psi_{ij}&=B_{ij}\exp\left[i\left(\xi x_1-\omega t\right)\right]\end{aligned} \tag{53}$$

where ξ is the wave number with units of 1/m, ω is the frequency with units of rad/s, and the coefficients A_i and B_{ij} represent wave amplitudes. Substituting these solutions into the decomposed set of equations of motion,

dispersion equations can be derived relating the frequency, ω, to the wave number, ξ. Thus, from Eqs. 48a and 48b, we get the following for uncoupled transverse shear waves

$$\frac{1}{3}\rho' d^2\omega^2 = b_2 + b_3 + (a_{10} + a_{13})\,\xi^2 \quad \text{Uncoupled Transverse Shear Waves} \tag{54}$$

From Eq. 48c, we get the following for uncoupled transverse rotational waves

$$\frac{1}{3}\rho' d^2\omega^2 = b_2 - b_3 + (a_{10} - a_{13})\,\xi^2 \quad \text{Uncoupled Transverse Rotational Wave} \tag{55}$$

Further from Eqs. 49 and 50, we get

$$\begin{vmatrix} k_{11}\xi^2 - \rho\omega^2 & k_{12}\xi & k_{13}\xi \\ k_{21}\xi & k_{22}\xi^2 + k'_{22} - \frac{1}{2}\rho' d^2\omega^2 & k_{23}\xi^2 \\ k_{31}\xi & k_{32}\xi^2 & k_{33}\xi^2 + k'_{33} - \rho' d^2\omega^2 \end{vmatrix} = 0; \quad \text{Longitudinal Waves} \tag{56}$$

and

$$\begin{vmatrix} \bar{k}_{11}\xi^2 - \rho\omega^2 & \bar{k}_{12}\xi & \bar{k}_{13}\xi \\ \bar{k}_{21}\xi & \bar{k}_{22}\xi^2 + \bar{k}'_{22} - \frac{2}{3}\rho' d^2\omega^2 & \bar{k}_{23}\xi^2 \\ \bar{k}_{31}\xi & \bar{k}_{32}\xi^2 & \bar{k}_{33}\xi^2 + \bar{k}'_{33} - \frac{2}{3}\rho' d^2\omega^2 \end{vmatrix} = 0; \quad \text{Transverse Waves} \tag{57}$$

By using Eqs. 43a–43c, the dispersion relationships can be obtained in terms of the micro-scale stiffness and length parameters. For example, Eqs. 54 and 55 will yield the following relationships

$$\omega^2 = \frac{l^2 N_p}{\rho' d^2}\left[\frac{2K_n^m + 3K_w^m}{5} + \left(\frac{2K_n^g + 12K_w^g}{35}l^2 + \frac{2G_n^u + 3G_w^u}{5}\right)\xi^2\right] \tag{58}$$

$$\omega^2 = \frac{l^2 N_p}{\rho' d^2}\left[K_w^m + \frac{4G_n^u + G_w^u}{5}\xi^2\right] \tag{59}$$

The explicit forms of dispersion relations for the case of longitudinal and transverse waves are not shown here due to their complexity. Numerical results for these cases will be presented later.

There are two distinct categories of waves: propagative waves and standing waves. Standing (evanescent) waves are waves for which the wave number is imaginary. These waves do not propagate through the material and just oscillate in a limited part of the material. Propagative waves for which the frequency is a real number are in turn categorized into two distinct types based on the value of their frequency cutoff defined at vanishing wave numbers (zero for acoustic waves and nonzero for optic waves). The frequency cutoffs are obtained from the dispersion equations, Eqs. 54–57, as follows

$$\begin{aligned} &\omega_{\xi=0} = \omega_{ns} \quad \text{Uncoupled transverse shear} \\ &\omega_{\xi=0} = \omega_s \quad \text{Uncoupled transverse rotational} \end{aligned} \tag{60}$$

$$\omega_{\xi=0} = \begin{cases} 0 \\ \omega_n \\ \omega_{ns} \end{cases}; \quad \text{Longitudinal} \qquad \omega_{\xi=0} = \begin{cases} 0 \\ \omega_{ns} \\ \omega_s \end{cases}; \quad \text{Transverse} \tag{61}$$

where

$$\omega_n = \sqrt{\left(\frac{l^2 N_p}{\rho' d^2}\right) K_n^m}; \quad \omega_s = \sqrt{\left(\frac{l^2 N_p}{\rho' d^2}\right) K_w^m}; \quad \omega_{ns} = \sqrt{\left(\frac{l^2 N_p}{\rho' d^2}\right) \frac{2K_n^m + 3K_w^m}{5}} \tag{62}$$

It should be noted that since normal stiffness coefficient is usually assumed to be higher than the tangential stiffness coefficient, the frequency cutoffs can be usually ordered as $0 < \omega_s < \omega_{ns} < \omega_n$. It is clearly seen that all branches of the uncoupled transverse waves are optical. The coupled waves (both the longitudinal and transverse) have one acoustic branch and two optical branches. It is noteworthy that the frequency cutoffs are functions of the stiffness components associated with the displacement gradient fluctuation, which is not included in classical first gradient continuum theories. By assigning the value of these stiffness coefficients, K_n^m and K_w^m, to be zero, it will be seen that all branches of all different wave types will turn into acoustic branches with frequency cutoffs equal to zero.

Now, taking derivatives of the equations governing the frequencies of the uncoupled transverse waves with respect to wave number, we get

$$\text{Shear} \quad \frac{\mathrm{d}\omega}{\mathrm{d}\xi} = \omega' = \sqrt{\frac{l^2 N_p}{\rho' d^2}} \frac{\left(\frac{2K_n^g + 12K_w^g}{35} l^2 + \frac{2G_n^u + 3G_w^u}{5}\right)\xi}{\sqrt{\frac{2K_n^m + 3K_w^m}{5} + \left(\frac{2K_n^g + 12K_w^g}{35} l^2 + \frac{2G_n^u + 3G_w^u}{5}\right)\xi^2}}$$

$$\text{Rotational} \quad \frac{\mathrm{d}\omega}{\mathrm{d}\xi} = \omega' = \sqrt{\frac{l^2 N_p}{\rho' d^2}} \frac{\frac{4G_n^u + G_w^u}{5}\xi}{\sqrt{K_w^m + \frac{4G_n^u + G_w^u}{5}\xi^2}} \tag{63}$$

The limit of the two equations as the wave number approaches infinity yields the constants that are the slopes of inclined asymptotes for the two dispersion graphs given as

$$\text{Shear} \quad \omega = \left(\sqrt{\frac{l^2 N_p}{\rho' d^2}\left(\frac{2K_n^g + 12K_w^g}{35} l^2 + \frac{2G_n^u + 3G_w^u}{5}\right)}\right)\xi$$

$$\text{Rotational} \quad \omega = \left(\sqrt{\frac{l^2 N_p}{\rho' d^2}\frac{4G_n^u + G_w^u}{5}}\right)\xi \tag{64}$$

It is observed from Eq. 63 that for vanishing rotational stiffness coefficients, G_n^u and G_w^u, the slope of the transverse rotational optic wave dispersion graph will be always zero. In this case, the medium will support transverse rotational optic waves of single frequency, ω_s. If in addition, the second gradient stiffness coefficients, K_n^g and K_w^g, also vanish, the slope of the shear wave will also be always identical to zero and the medium will only support transverse shear optic wave of single frequency, ω_{ns}.

8 Results and discussions

To illustrate the relationship between the micro-scale parameters and the dispersion behavior, a parametric study is performed by varying the ratios of tangential to normal inter-granular stiffness parameters defined in Eq. 44. Dispersion plots showing the wave propagation frequencies versus the wave number for the eight different waves (3 longitudinal, 3 transverse waves, and the 2 uncoupled transverse shear and rotational waves) are presented in Fig. 3 for ratios of tangential to normal stiffness parameters ranging from 0 to 1. These calculations are performed for the micro-scale parameters and the resultant macroscopic parameters as given in Table 1, which could represent a hard to medium hard granular rock. The average grain size, l, has been assumed to be 1 mm, and the micro-volume is assumed to be composed of a grain and its immediate neighbors such that, $d = 1$ mm. For the assumed average grain size, the number of grain-pair interactions, N_p, is estimated. Figure 3a–d, show the effect of variation of ratios β_M, β_m, β_g, and β_G, respectively, while keeping all other parameters constant. For the set of parameters as proposed in Table 1, we see a rather unique dispersion behavior characterized by distinct band gaps over a wide range of wave numbers. To refrain from adding further clutter in Fig. 3, the specific band gaps, especially those for which no kind of waves can propagate, are shown later in Fig. 4. From Fig. 3, it is seen that, in general, longitudinal waves include two optic branches with frequency cutoffs equal to ω_n and ω_{ns} and an acoustic branch. Typically, transverse waves also have two optic branches with cutoffs of ω_s and ω_{ns} along with an acoustic branch, while the uncoupled waves consist of two optical waves with frequency cutoffs of ω_s and ω_{ns}. There is an exception for the case of $\beta_m = 0$ which implies that frequency cutoff $\omega_s = 0$ leading to one less optical branch for both transverse and uncoupled waves. The dispersion behavior of longitudinal and transverse waves (Fig. 3a1–d1, a2–d2) is similar characterized by (1) an optical branch, which has a nonlinear monotonically increasing curve starting from a higher-frequency cutoff; (2) a second optical branch beginning at lower-frequency cutoff, which shows initial increase before reaching an asymptote; and (3) an acoustic branch which is an increasing function prior to reaching an asymptote. The uncoupled waves are typically characterized by optical wave with a weak dependency upon wavenumber. This is expected since the coefficient multiplying the wave number is composed of only stiffness parameters associated with the second gradient and the rotation terms (see Eqs. 58 and 59), which are significantly smaller than the other stiffness measures.

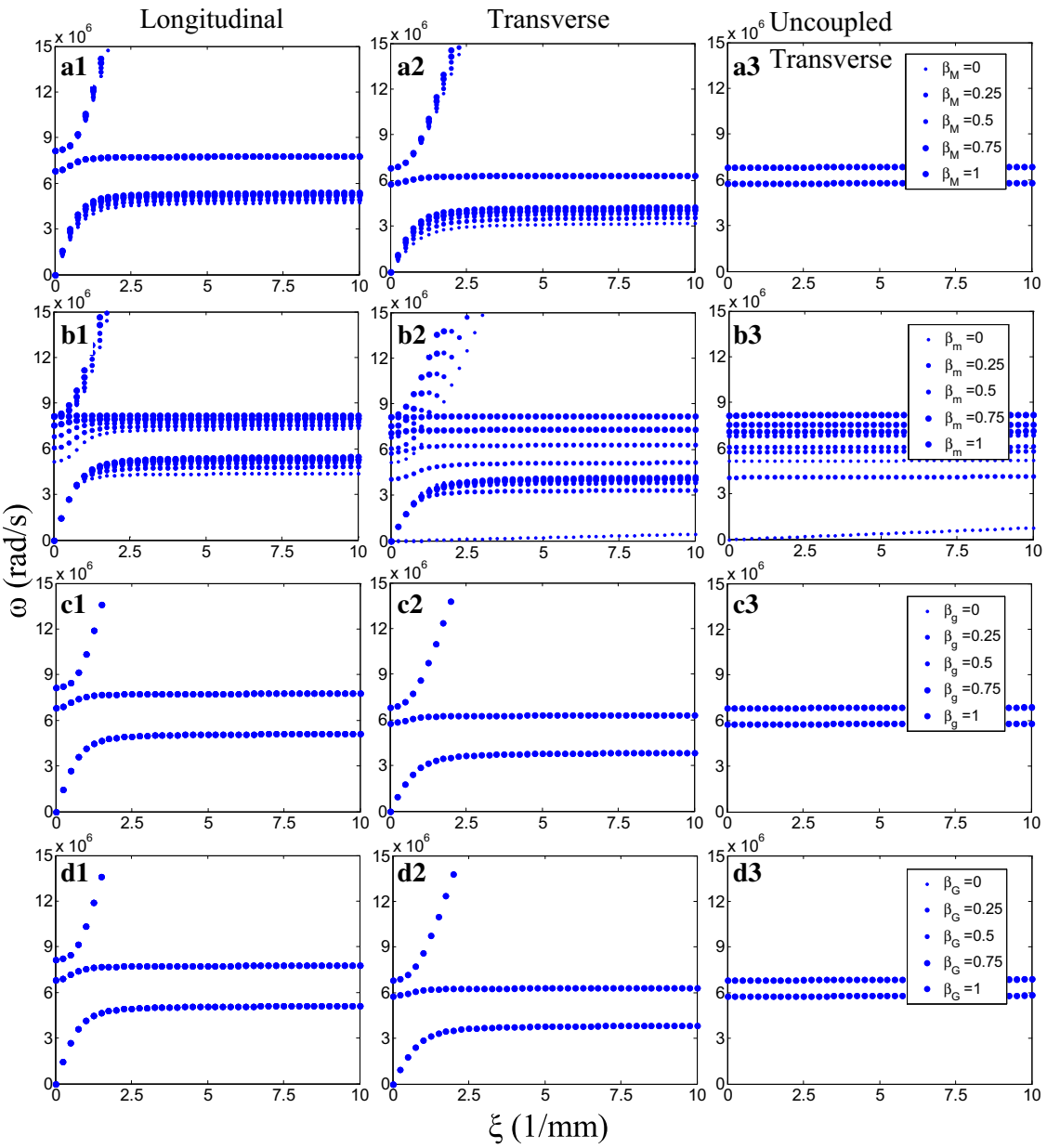

Fig. 3 Dispersion behavior of longitudinal waves (**a1**–**d1**), transverse waves (**a2**–**d2**), and uncoupled transverse shear and rotational waves (**a3**–**d3**). Dispersion graphs are given for different ratios between normal and tangential components of the micro-scale stiffness parameters

It is interesting to note that there are regions in the frequency domain where none of the three distinct wave categories show the existence of a wave number, which is non-imaginary. Thus, for the set of parameters proposed in Table 1, complete band gap exists as none of the waves can propagate through the material. Figure 3a1, a2 show that the stiffness components associated with the average displacement gradient field change only the value of the asymptotes of the acoustic branches. Figure 3 also shows that the dispersion behavior and the predicted band-gap phenomena are most affected by the tangential component of the intergranular stiffness parameter related to fluctuations (see the effect of β_m in Fig. 3b1, b3). When the tangential stiffness coefficient is zero ($\beta_m = 0$), for both the coupled and uncoupled transverse waves, the dispersion curve for acoustic branch is linearly increasing, implying that at all frequencies we have non-imaginary wave number ruling out the possibility of a band gap. In this case, the skew-symmetric part of C^m_{ijkl} vanishes or equivalently for Mindlin moduli $b_1 (= b_3) = b_2$. The situation is similar to the case in which, μ_c, in the recently

Table 1 Micro-scale parameters (left) and the corresponding macro-scale constitutive parameters (right)

Model parameters	Values	Macroscopic parameters	Values
l	10^{-3} m	λ	6.67 GPa
d	10^{-3} m	μ	23.33 GPa
N_p	10^9 1/m^3	E	51.85 GPa
ρ'	3000 Kg/m^3	ν	0.111
ρ	1570 Kg/m^3	$b_1 = b_3$	6.67 GPa
K_n^M	200 MN/m	b_2	40.00 GPa
β_M	0.5	A^g_{111111}	2.29×10^{-6} MN
K_n^m	200 MN/m	A^g_{111122}	9.52×10^{-7} MN
β_m	0.5	A^g_{111221}	9.52×10^{-8} MN
K_n^g	2×10^{-2} MN/m	A^g_{122122}	7.62×10^{-7} MN
β_g	0.5	A^u_{121121}	4.00×10^{-6} MN
G_n^u	2×10^{-8} N.m	A^u_{132132}	4.67×10^{-6} MN
β_G	0.5	A^u_{121233}	6.67×10^{-7} MN

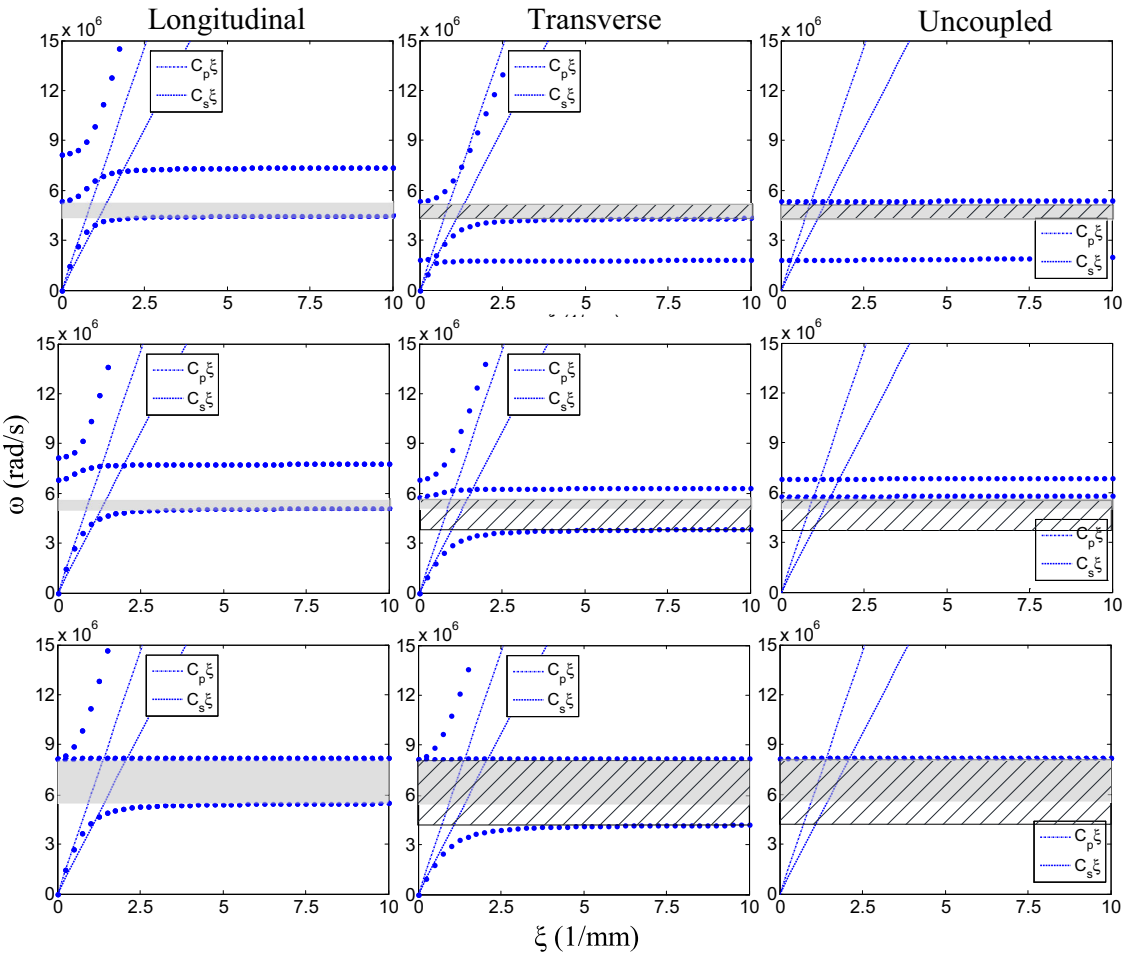

Fig. 4 Dispersion behavior of longitudinal, transverse, and uncoupled tr ansverse waves for $\beta_m = 0.05$ (**a1–a3**), $\beta_m = 0.05$ (**b1–b3**), and $\beta_m = 1.0$ (**c1–c3**)

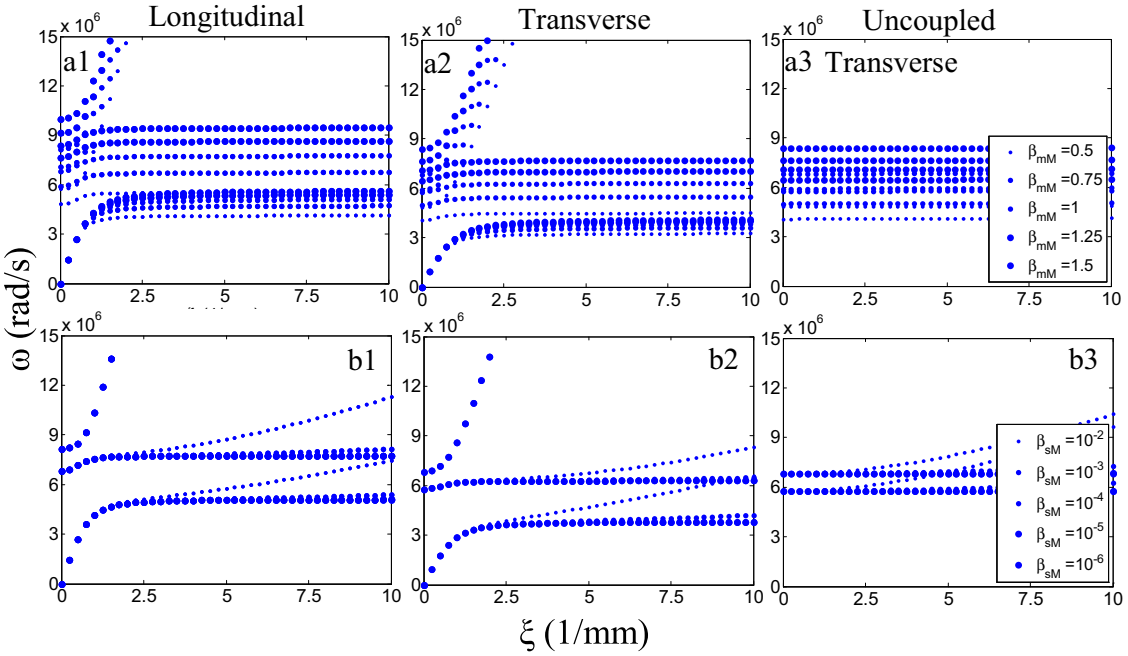

Fig. 5 Microstructural effects upon the dispersion behavior of longitudinal, transverse, and uncoupled transverse waves

proposed relaxed linear micromorphic model vanishes [46,47]. The results obtained are similar in this case to those given in [45] for $\mu_c = 0$. However, as β_m becomes nonzero, an additional optic branch instead of the acoustic branch appears for both the coupled and uncoupled transverse waves. Further, above a certain value of β_m, band gap appears. These effects are exemplified in Fig. 4, where we have separately shown the dispersion curves for $\beta_m = 0.05$, 0.5, and 1.0. As reference, the classical compressive, P, and shear, S, waves are also included in Fig. 4 using

$$\omega_P = C_p\xi = \left(\sqrt{\frac{\lambda + 2\mu}{\rho}}\right)\xi; \quad \omega_S = C_s\xi = \left(\sqrt{\frac{\mu}{\rho}}\right)\xi \tag{65}$$

The band gap for which no kind of waves can propagate is shown by the shaded region in Fig. 4. In addition, band gap for transverse waves is shown by the hatched region. Clearly, the band-gap region changes with β_m. For $\beta_m = 0.05$ and 1.0, the frequency region between the maximum value of the acoustic branch of the transverse waves and ω_s represents a band gap for all transverse waves, coupled and uncoupled. For $\beta_m = 1.0$, the two optical branches of the longitudinal waves, transverse coupled waves, and transverse uncoupled waves all have the same frequency cutoff, and their dispersion graphs show monotonically increasing curves. The acoustic branches of the longitudinal and the coupled transverse waves have clear horizontal asymptote, which is smaller than the nonzero frequency cutoff. The region between the horizontal asymptote of the longitudinal wave and the nonzero frequency cutoff is a complete band-gap region. It is noteworthy that optical rotational and transverse waves as well as frequency band gaps have been observed both in experiments and in discrete models of regular hexagonal closed-paced grain packing [48,49]. Further, frequency band gaps have been predicted for elastic metamaterials with resonators [50].

The microstructural effects upon dispersion behavior are further illustrated parametrically by varying the following ratios dealing with the fluctuation, second gradient, and rotational inter-granular stiffness parameters

$$\beta_{mM} = \frac{K_n^m}{K_n^M} = \frac{K_w^m}{K_w^M}; \quad \beta_{sM} = \frac{K_n^g}{K_n^M} = \frac{K_w^g}{K_w^M} = \frac{G_n^u}{l^2 K_n^M} = \frac{G_w^u}{l^2 K_w^M} \tag{66}$$

The ratio, β_{mM}, is varied between 0.50 and 1.50, while the remaining parameters kept same as in Table 1. Figure 5a1–a3 gives the resultant variation in dispersion behavior. In all these cases, dispersion behavior is similar with a characteristic band gap over the computed wave number range. The size of band gap increases with β_{mM}; the frequency cutoff of the optical branches is particularly affected since they depend upon the

fluctuation-related inter-granular stiffness. Furthermore, since K_n^m and K_w^m represent the stiffness related to fluctuations caused by the microstructure, larger β_{mM} implies a larger effect of microstructure. Figure 5b1–b3 gives the effect of varying β_{sM} between 10^{-2} and 10^{-6}. Again all the remaining parameters are kept same as those in Table 1. The ratio β_{sM} is related to the influence of characteristic length-scale associated with second gradient moduli; thus, larger β_{sM} implies stronger long-range effect. In this case, the initial cutoff frequencies do not change, however, the band gap disappears for larger β_{sM}. Thus, for strongly second gradient media, no band gap will be observed, which agrees with the finding by Madeo et al. [45].

9 Summary and conclusion

The granular micromechanics approach has been applied to find a micromorphic continuum model for elasticity of granular media. In this approach, continuum model of granular material is obtained by considering the interactions of grain pairs. Since the complete granular microstructure and micromechanics of a material are seldom known, it is impossible to know the displacement field of all the grains within a material point. In this paper, we have adopted the kinematic analyses of Mindlin–Eringen microstructural elasticity or micromorphic mechanics. As a result, the relative displacement of interacting grain pairs is decomposed into an average term compatible with the macro-scale field, a micro-scale fluctuation term defined within a material point, and its second gradient. In addition, the second gradient terms are found to give rise to relative rotations between grain pairs. The macro-scale deformation energy density is thus modeled as a summation of micro-scale deformation energy defined for each grain-pair as a function of inter-granular relative displacements and rotations. Consequently, inter-granular force conjugates are defined for each micro-scale kinematic measure and the macro-scale stress conjugates are obtained in terms of these inter-granular forces. Furthermore, for linear elasticity, the micro-scale deformation energy is formulated as a quadratic function of the kinematic measures, which requires introduction of four different inter-granular stiffness measures. The macro-scale constitutive relationship is then obtained in terms of these inter-granular stiffness measures. These relationships are shown to be consistent with Mindlin–Eringen model, and the constitutive coefficients of Mindlin's model are identified in terms of the inter-granular stiffness parameters. We note that the coupling between different strain and stress has been neglected here and might be topics of future work.

The derived model is applied to investigate wave propagation phenomena. Dispersion graphs for different cases and different ratios between the microscopic stiffness parameters have been presented. It is seen that the model has the capability to present band gaps over a large range of wave numbers. In most cases, there is a complete band gap in the frequency domain, wherein for none of the three wave categories (Longitudinal, transverse, and uncoupled transverse), there exists a non-imaginary value for the wave number. It is shown that the frequency cutoffs in the dispersion graphs which define whether the waves are optical or acoustic are only functions of the stiffness parameters associated with the fluctuations in displacement gradient. Consequently, in classical continuum where the fluctuations in displacement and their associated stiffness components are ignored, all waves will be of acoustic type and there will be no possibility of frequency band gaps. Furthermore, for relatively large values of stiffness measures associated with second gradient terms, the band gaps also vanish. It is noteworthy, however, that second gradient terms are necessary for modeling some frequency dependent wave transmission/reflection phenomena at material interfaces [51,52]. The calculations shown in this paper indicate the possibility of designing materials with specific wave propagation behaviors that can be used as alternates to piezoelectric materials used commonly for structural vibration control [53–59] or for damage identification [60–62]. Alternatively, such materials can be applied to help the optimal control procedures [63,64] or for optimal biomaterial design [65] in bone mechanics. The granular micromechanics-based micromorphic model derived here or its micropolar and second gradient simplifications can also be used to describe post-instability macro-scale behavior, such as boundary and localization layers in microstructured media [66,67].

Acknowledgments This research was supported in part by the United States National Science Foundation Grant CMMI-1068528.

References

1. Cosserat, E., Cosserat, F.: Theory of Deformable Bodies. Scientific Library A. Hermann and Sons, Paris (1909)
2. Mindlin, R.D.: Micro-structure in linear elasticity. Arch. Ration. Mech. Anal. **16**(1), 51–78 (1964)
3. Toupin, R.A.: Theories of elasticity with couple-stress. Arch. Ration. Mech. Anal. **17**(2), 85–112 (1964)

4. Eringen, A.C.: Microcontinuum Field Theories: Foundations and Solids. Springer, New York (1999)
5. Green, A.E., Rivlin, R.S.: Multipolar continuum mechanics. Arch. Ration. Mech. Anal. **17**(2), 113–147 (1964)
6. Germain, P.: Method of virtual power in continuum mechanics. 2. Microstructure. SIAM J. Appl. Math. **25**(3), 556–575 (1973). doi:10.1137/0125053
7. Navier, C.L.: Sur les lois de l'equilibre et du mouvement des corps solides elastiques. Memoire de l'Academie Royale Sci. **7**, 375–393 (1827)
8. Cauchy, A.-L.: Sur l'equilibre et le mouvement d'un systeme de points materiels sollicites par des forces d'attraction ou de repulsion mutuelle. Excercises de Mathematiques 3:188–212 (1826–1830)
9. dell'Isola, F., Andreaus, U., Placidi, L.: At the origins and in the vanguard of peri-dynamics, non-local and higher gradient continuum mechanics. An underestimated and still topical contribution of Gabrio Piola. Mech. Math. Solids (2013). doi:10.1177/1081286513509811
10. Auffray, N., dell'Isola, F., Eremeyev, V., Madeo, A., Rosi, G.: Analytical continuum mechanics á la Hamilton-Piola: least action principle for second gradient continua and capillary fluids. Math. Mech. Solids (2013, accepted)
11. Nguyen, V.P., Stroeven, M., Sluys, L.J.: Multiscale continuous and discontinuous modeling of heterogeneous materials: a review on recent developments. J. Multiscale Model. **3**(04), 229–270 (2011)
12. Placidi, L., Hutter, K.: Thermodynamics of polycrystalline materials treated by the theory of mixtures with continuous diversity. Continuum Mech. Thermodyn. **17**(6), 409–451 (2006)
13. Placidi, L., Greve, R., Seddik, H., Faria, S.H.: Continuum-mechanical, anisotropic Flow model for polar ice masses, based on an anisotropic flow enhancement factor. Continuum Mech. Thermodyn. **22**(3), 221–237 (2010)
14. Misra, A., Singh, V.: Nonlinear granular micromechanics model for multi-axial rate-dependent behavior. Int J Solids Struct. (2014). doi:10.1016/j.ijsolstr.2014.02.034
15. Misra, A., Singh, V.: Thermomechanics based nonlinear rate-dependent coupled damage-plasticity granular micromechanics model. Continuum Mech. Thermodyn. (2014). doi:10.1007/s00161-014-0360-y
16. Misra, A., Poorsolhjouy, P.: Granular micromechanics model for damage and plasticity of cementitious materials based upon thermomechanics. Math. Mech. Solids (2015). doi:10.1177/1081286515576821
17. Chang, C.S., Misra, A.: Theoretical and experimental-study of regular packings of granules. J. Eng. Mech. ASCE **115**(4), 704–720 (1989)
18. Chang, C.S., Misra, A.: Packing structure and mechanical-properties of granulates. J. Eng. Mech. ASCE **116**(5), 1077–1093 (1990)
19. Digby, P.J.: The effective elastic moduli of porous granular rocks. J. Appl. Mech. **48**, 803–808 (1981)
20. Walton, K.: The effective elastic moduli of a random packing of spheres. J. Mech. Phys. Solids **35**, 213–226 (1987)
21. Deresiewicz, H.: Stress-strain relations for a simple model of a granular medium. J. Appl. Mech. **25**, 402–406 (1958)
22. Duffy, J., Mindlin, R.D.: Stress-strain relations of a granular medium. J. Appl. Mech. **24**(4), 585–893 (1957)
23. Chang, C.S., Hicher, P.Y.: An elasto-plastic model for granular materials with microstructural consideration. Int. J. Solids Struct. **42**(14), 4258–4277 (2005). doi:10.1016/j.ijsolstr.2004.09.021
24. Placidi, L.: A variational approach for a nonlinear one-dimensional damage-elasto-plastic second-gradient continuum model. Continuum Mech. Thermodyn. 1–19 (2014). doi:10.1007/s00161-014-0405-2
25. Misra, A., Poorsolhjouy, P.: Micro-macro scale instability in 2D regular granular assemblies. Continuum Mech. Thermodyn. **27**(1–2), 63–82 (2013). doi:10.1007/s00161-013-0330-9
26. Chang, C.S., Yin, Z.Y., Hicher, P.Y.: Micromechanical analysis for interparticle and assembly instability of sand. J. Eng. Mech. ASCE. **137**(3), 155–168 (2011)
27. Chang, C.S., Gao, J.: 2nd-gradient constitutive theory for granular material with random packing structure. Int. J. Solids Struct. **32**(16), 2279–2293 (1995)
28. Suiker, A.S.J., de Borst, R., Chang, C.S.: Micro-mechanical modelling of granular material. Part 1: derivation of a second-gradient micro-polar constitutive theory. Acta Mech. **149**(1–4), 161–180 (2001)
29. Yang, Y., Misra, A.: Micromechanics based second gradient continuum theory for shear band modeling in cohesive granular materials following damage elasticity. Int. J. Solids Struct. **49**(18), 2500–2514 (2012). doi:10.1016/j.ijsolstr.2012.05.024
30. Misra, A., Chang, C.S.: Effective elastic moduli of heterogeneous granular solids. Int. J. Solids Struct. **30**(18), 2547–2566 (1993)
31. Agnolin, I., Jenkins, J.T., La Ragione, L.: A continuum theory for a random array of identical, elastic, frictional disks. Mech. Mater. **38**(8–10), 687–701 (2006)
32. Misra, A., Jiang, H.: Measured kinematic fields in the biaxial shear of granular materials. Comput. Geotech. **20**(3–4), 267–285 (1997). doi:10.1016/S0266-352x(97)00006-2
33. Richefeu, V., Combe, G., Viggiani, G.: An experimental assessment of displacement fluctuations in a 2D granular material subjected to shear. Geotech. Lett. **2**, 113–118 (2012). doi:10.1680/geolett.12.00029
34. Misra, A.: Particle Kinematics in Sheared Rod Assemblies Physics of Dry Granular Media. pp. 261–266. Springer, Berlin (1998)
35. Jenkins, J., Johnson, D., La Ragione, L., Makse, H.: Fluctuations and the effective moduli of an isotropic, random aggregate of identical, frictionless spheres. J. Mech. Phys. Solids **53**(1), 197–225 (2005)
36. Alibert, J.J., Seppecher, P., Dell'Isola, F.: Truss modular beams with deformation energy depending on higher displacement gradients. Math. Mech. Solids **8**(1), 51–73 (2003). doi:10.1177/108128603029658
37. Seppecher, P., Alibert, J.-J., dell'Isola, F.: Linear elastic trusses leading to continua with exotic mechanical interactions. J. Phys. Conf. Ser. **319**(1), 012018 (2011)
38. Andreaus, U., Giorgio, I., Lekszycki, T.: A 2-D continuum model of a mixture of bone tissue and bio-resorbable material for simulating mass density redistribution under load slowly variable in time. ZAMM-Z Angew Math Me **94**(12), 978–1000 (2014)
39. Andreaus, U., Chiaia, B., Placidi, L.: Soft-impact dynamics of deformable bodies. Continuum Mech. Thermodyn. **25**(2–4), 375–398 (2013)

40. Andreaus, U., Placidi, L., Rega, G.: Microcantilever dynamics in tapping mode atomic force microscopy via higher eigenmodes analysis. J. Appl. Phys. **113**(22) (2013)
41. Kanatani, K.I.: Distribution of directional-data and fabric tensors. Int. J. Eng. Sci. **22**(2), 149–164 (1984)
42. Mardia, K.V., Jupp, P.E.: Directional Statistics. Wiley, New York (2009)
43. dell'Isola, F., Sciarra, G., Vidoli, S.: Generalized Hooke's law for isotropic second gradient materials. Proc. R. Soc. Math. Phys. Eng. Sci. **465**(2107), 2177–2196 (2009). doi:10.1098/rspa.2008.0530
44. Love, A.E.H.: A Treatise on the Mathematical Theory of Elasticity. Dover, New York (1944)
45. Madeo, A., Neff, P., Ghiba, I.-D., Placidi, L., Rosi, G.: Wave propagation in relaxed micromorphic continua: modeling metamaterials with frequency band-gaps. Continuum Mech. Thermodyn. 1–20 (2013). doi:10.1007/s00161-013-0329-2
46. Ghiba, I.-D., Neff, P., Madeo, A., Placidi, L., Rosi, G.: The relaxed linear micromorphic continuum: existence, uniqueness and continuous dependence in dynamics. Math. Mech. Solids. arXiv preprint arXiv:1308.3762 (2013). doi:10.1177/1081286513516972
47. Neff, P., Ghiba, I.-D., Madeo, A., Placidi, L., Rosi, G.: A unifying perspective: the relaxed linear micromorphic continuum. Continuum Mech. Thermodyn. **26**(5), 639–681 (2013). doi:10.1007/s00161-013-0322-9
48. Merkel, A., Tournat, V., Gusev, V.: Dispersion of elastic waves in three-dimensional noncohesive granular phononic crystals: properties of rotational modes. Phys. Rev. E **82**(3) (2010)
49. Merkel, A., Tournat, V., Gusev, V.: Experimental evidence of rotational elastic waves in granular phononic crystals. Phys. Rev. Lett. **107**(22) (2011)
50. Zhu, R., Huang, H.H., Huang, G.L., Sun, C.T.: Microstructure continuum modeling of an elastic metamaterial. Int. J. Eng. Sci. **49**(12), 1477–1485 (2011)
51. Placidi, L., Rosi, G., Giorgio, I., Madeo, A.: Reflection and transmission of plane waves at surfaces carrying material properties and embedded in second-gradient materials. Math. Mech. Solids. **19**(5), 555–578 (2014)
52. dell'Isola, F., Madeo, A., Placidi, L.: Linear plane wave propagation and normal transmission and reflection at discontinuity surfaces in second gradient 3D continua. ZAMM-Z Angew Math Me. **92**(1), 52–71 (2012). doi:10.1002/zamm.201100022
53. Maurini, C., dell'Isola, F., Pouget, J.: On models of layered piezoelectric beams for passive vibration control. J. Phys. IV **115**, 307–316 (2004)
54. Maurini, C., Pouget, J., dell'Isola, F.: Extension of the Euler–Bernoulli model of piezoelectric laminates to include 3D effects via a mixed approach. Comput. Struct. **84**(22–23), 1438–1458 (2006)
55. Porfiri, M., dell'Isola, F., Santini, E.: Modeling and design of passive electric networks interconnecting piezoelectric transducers for distributed vibration control. Int. J. Appl. Electrom. **21**(2), 69–87 (2005)
56. Vidoli, S., dell'Isola, F.: Vibration control in plates by uniformly distributed PZT actuators interconnected via electric networks. Eur. J. Mech. A-Solids **20**(3), 435–456 (2001)
57. Madeo, A., Placidi, L., Rosi, G.: Towards the design of metamaterials with enhanced damage sensitivity: second gradient porous materials. Res. Nondestruct. Eval. **25**(2), 99–124 (2014)
58. dell'Isola, F., Vidoli, S.: Continuum modelling of piezoelectromechanical truss beams: an application to vibration damping. Arch. Appl. Mech. **68**(1), 1–19 (1998)
59. Greco, L., Impollonia, N., Cuomo, M.: A procedure for the static analysis of cable structures following elastic catenary theory. Int. J. Solids Struct. **51**(7–8), 1521–1533 (2014)
60. Andreaus, U., Baragatti, P.: Cracked beam identification by numerically analysing the nonlinear behaviour of the harmonically forced response. J. Sound Vib. **330**(4), 721–742 (2011)
61. Andreaus, U., Baragatti, P.: Experimental damage detection of cracked beams by using nonlinear characteristics of forced response. Mech. Syst. Signal Process. **31**, 382–404 (2012)
62. Ferretti, M., Madeo, A., Dell'Isola, F., Boisse, P.: Modeling the onset of shear boundary layers in fibrous composite reinforcements by second-gradient theory. Zeitschrift für Angewandte Mathematik Und Physik **65**(3), 587–612 (2014)
63. Andreaus, U., Colloca, M., Iacoviello, D.: An optimal control procedure for bone adaptation under mechanical stimulus. Control Eng. Pract. **20**(6), 575–583 (2012)
64. Andreaus, U., Colloca, M., Iacoviello, D.: Optimal bone density distributions: numerical analysis of the osteocyte spatial influence in bone remodeling. Comput. Methods Programs Biomed. **113**(1), 80–91 (2014)
65. Andreaus, U., Giorgio, I., Madeo, A.: Modeling of the interaction between bone tissue and resorbable biomaterial as linear elastic materials with voids. Zeitschrift für angewandte Mathematik und Physik 1–29 (2014)
66. Altenbach, H., Eremeyev, V.A., Lebedev, L.P., Rendon, L.A.: Acceleration waves and ellipticity in thermoelastic micropolar media. Arch. Appl. Mech. **80**(3), 217–227 (2010). doi:10.1007/s00419-009-0314-1
67. Placidi, L.: A variational approach for a nonlinear 1-dimensional second gradient continuum damage model. Continuum Mech. Thermodyn. 1–16 (2014). doi:10.1007/s00161-014-0338-9